Energy & Environmental Science

Cite this: *Energy Environ. Sci.*, 2012, **5**, 7936

www.rsc.org/ees

**PAPER**

# Exploration of the active center structure of nitrogen-doped graphene-based catalysts for oxygen reduction reaction†

**Linfei Lai,[abc] Jeffrey R. Potts,[b] Da Zhan,[a] Liang Wang,[a] Chee Kok Poh,[c] Chunhua Tang,[d] Hao Gong,[d] Zexiang Shen,[a] Jianyi Lin[c] and Rodney S. Ruoff*[b]**

***Received 30th March 2012, Accepted 25th April 2012***
**DOI: 10.1039/c2ee21802j**



We present two different ways to fabricate nitrogen-doped graphene (N-graphene) and demonstrate its use as a metal-free catalyst to study the catalytic active center for the oxygen reduction reaction (ORR). N-graphene was produced by annealing of graphene oxide (G-O) under ammonia or by annealing of a N-containing polymer/reduced graphene oxide (RG-O) composite (polyaniline/RG-O or polypyrrole/RG-O). The effects of the N precursors and annealing temperature on the performance of the catalyst were investigated. The bonding state of the N atom was found to have a significant effect on the selectivity and catalytic activity for ORR. Annealing of G-O with ammonia preferentially formed graphitic N and pyridinic N centers, while annealing of polyaniline/RG-O and polypyrrole/RG-O tended to generate pyridinic and pyrrolic N moieties, respectively. Most importantly, the electrocatalytic activity of the catalyst was found to be dependent on the graphitic N content which determined the limiting current density, while the pyridinic N content improved the onset potential for ORR. However, the total N content in the graphene-based non-precious metal catalyst does not play an important role in the ORR process.

## Introduction

Fuel cells are considered to be a promising green energy generation technology; however, the high cost of the catalyst, the inherent oxygen crossover from anode to cathode, and sluggish oxygen reduction reaction (ORR) kinetics at the cathode hinder their widespread commercialization.[1,2] Traditionally, the catalyst cathode consists of Pt nanoparticles supported on high surface area carbon composites. Recent investigations of alternative non-noble ORR catalysts include catalysts based on transition metal chalcogenides,[3] N-doped carbon nanomaterials,[4,5] and N-containing polymer/metal chelates.[6] In the latter case, several reports have found that the transition metal itself does not function as an active site for ORR, but rather facilitates the incorporation of active N-containing functionalities into graphitic carbons at high temperature.[6,7] Several research groups have reported enhanced ORR activities on N-doped carbon nanomaterials, where pyridinic N at the carbon edge plane helps the reduction of oxygen.[8,9]

Very recently, metal-free N-doped carbons have been reported to exhibit ORR catalytic activities superior to commercial Pt/C catalysts,[10,11] representing a breakthrough for metal-free, N-containing catalysts and their use in applications such as metal–air batteries and fuel cells. For example, N-doped CNTs display higher catalytic activity than traditional Pt/C due to the

[a]*Division of Physics and Applied Physics, School of Physical and Mathematical Sciences, Nanyang Technological University, 637371, Singapore*
[b]*Department of Mechanical Engineering and the Materials Science and Engineering Program, University of Texas at Austin, One University Station C2200, Austin, TX 78712, USA. E-mail: r.ruoff@mail.utexas.edu*
[c]*Institute of Chemical and Engineering Sciences, A*STAR, 1 Pesek Road, Jurong Island, 627833, Singapore*
[d]*Department of Materials Science and Engineering, National University of Singapore, 117576, Singapore*

† Electronic supplementary information (ESI) available: The linear voltammetric curves and Koutecky–Levich plots of different catalysts. See DOI: 10.1039/c2ee21802j

### Broader context

Metal-free N-doped carbons have been reported to exhibit oxygen reduction reaction (ORR) catalytic activity, indicating their potential as a catalyst for fuel cells and metal air batteries. However, the nature of the catalytic center of N-doped carbon has not been clearly understood. We reacted graphene oxide (G-O) with different N-containing precursors (ammonia gas and N-containing polymers) to prepare N-doped chemically modified graphene. The degree and type of N doping can be tuned by the annealing temperature and the type of N precursor. The electrocatalytic activity of the catalyst was found to be dependent on the graphitic N content which determined the limiting current density, while the pyridinic N content improved the onset potential for ORR.

presence of pyridinic and pyrrolic N species.[12,13] N-graphene prepared using a chemical vapor deposition (CVD) method has shown a high electrocatalytic activity toward ORR, with a limiting current density three times larger than 20 wt% Pt/C; this improvement in ORR activity was attributed to the pyridinic N-abundant structure.[10] Similar conclusions have been reported by other researchers.[14,15] Pyridinic N, which possesses one lone pair of electrons in addition to the electron donated to the conjugated $\pi$ bond, facilitates reductive $O_2$ adsorption and therefore may be catalytic active.[16] We also have used a CVD method to produce N-doped graphene with pyridinic-N as the dominant dopant; however, we found that the as-prepared N-doped graphene does not show remarkable ORR catalytic ability as previously reported.[17] Therefore, pyridinic N content may not be the key parameter determining the ORR catalytic activity. Wang *et al.* reported that introduction of N to the carbon network would improve its ORR activity, because the electronic density of states near the Fermi level of the N-doped carbon increased.[18] N, especially the graphitic N atoms in the carbon lattice, facilitated electron transfer from the carbon electronic bands to the antibonding orbitals of $O_2$.[18] Recently, Kim *et al.* proposed that N-doped edge structures, in particular graphitic N sites, gave the most pronounced ORR activity improvement.[19] In light of these conflicting results, it is therefore reasonable and important to identify the active sites of nonmetal-based ORR catalysts for better understanding of the reduction mechanism.

Using a CVD approach, pyridinic-N-doped graphene can be produced easily in a simple, one-step process. However, the type of N-containing groups formed on graphene cannot be varied simply by adjusting the reaction time and temperature. To alter the identities of the N moieties we used chemically prepared graphene oxide (G-O) and different N-containing precursors (ammonia gas and N-containing polymers) as the starting materials for preparation of N-doped graphene. Using chemically derived G-O as the precursor carbon, it was found that the N doping state can indeed be effectively tuned by controlling annealing temperature and by judicious selection of the N precursor. Polyaniline (PANi) and polypyrrole (Ppy)/G-O composites with N contents of over 10 at% N were annealed at 850 °C and will be referred to as PANi/RG-O and Ppy/RG-O, respectively (RG-O indicates reduction of G-O to reduced graphene oxide during the annealing process). N-doped RG-O prepared by annealing of G-O powder under different temperatures ranging from 550 to 1000 °C, together with PANi/RG-O and Ppy/RG-O, was used as the catalyst to investigate the effect of the N doping state as well as the effect of the total N content in the graphene composite on ORR performance. The ORR performance of N-doped graphene with different N-containing groups is thus presented herein. The motivation of this research was to perform a mechanistic study on the ORR active sites of N-doped graphene, to better understand the relationship between the structure of the N dopant species and catalytic activity.

## Experimental

### Preparation of G-O

GO was prepared from natural flake graphite powder as reported elsewhere.[20] 5 g of graphite and 3.5 g of $NaNO_3$ were placed in a flask. The flask was put on an ice bath and 350 mL of $H_2SO_4$ was added to the flask, followed by 10 g of $KMnO_4$ and stirred vigorously for 2 hours. The flask was then taken off the ice bath and kept at room temperature for 6 days. Then 200 mL of 5 wt% $H_2SO_4$ was added to the mixture, and the mixture was kept at 98 °C for 2 hours. The temperature was decreased to 50 °C and 10 mL of $H_2O_2$ (30 wt% aqueous solution) was added to terminate the reaction. The resultant mixture was purified by washing with 1 L of 3 wt% $H_2SO_4$–$H_2O$ mixture followed by centrifugation (6000 rpm for 20 min) until the supernatant was colorless with a pH value around 6.5. G-O was produced by exfoliating GO in water (1 mg $mL^{-1}$) by ultrasonication for one hour. The G-O was collected and freeze dried for further use.

### Preparation of N-doped RG-O

N-doped RG-O was prepared by annealing of G-O powder at temperatures of 550 °C, 850 °C, and 1000 °C under $NH_3$, and is henceforth labeled as N-RG-O 550 °C, N-RG-O 850 °C, and N-RG-O 1000 °C, respectively. Briefly, 500 mg of G-O powder was put in a tube furnace under a flow of 5% $NH_3$ in Ar (50 sccm) and annealed for one hour after reaching the desired annealing temperature. The resulting sample was ground and washed repeatedly with distilled water and dried at 60 °C for 24 h.

*Boron (B)- and N-doped RG-O (BN-RG-O) preparation*: the N-RG-O 550 °C sample was ground by mortar with $H_3BO_3$ and annealed at 1000 °C for 1 h under flowing Ar (50 sccm). The resulting sample was ground and washed repeatedly with distilled water and dried at 60 °C for 24 h for further use.

*Ppy/RG-O composite preparation*: pyrrole was distilled twice before use. 20 mg of G-O powder was ultrasonically dispersed in 20 mL of DI water and 1.5 mL of 0.1 M pyrrole in methanol was subsequently added dropwise to the mixture. After 10 min, 0.662 mL of 1 M $FeCl_3$ was added dropwise over the course of 10 min. The solution was shielded from light and kept in an ice bath, with magnetic stirring for 8 h for polymerization. The product was washed with ethanol and acetone to remove the residual oxidant, followed by rinsing several times with a large amount of water. The loading of polypyrrole in the composite was ~50 wt%, and the total N content in the Ppy/G-O composite was ~10.4 wt%. After drying at 60 °C, the resulting product was annealed at 850 °C under Ar protection (50 sccm) for 1 h, and washed by ethanol, then DI water for further use. The sample is labeled as Ppy/RG-O.

*PANi/RG-O composite preparation*: the aniline monomer was distilled twice before use. 20 mg of G-O was ultrasonically dispersed in 20 mL of DI water; 1.54 mL of 0.1 M aniline was then added dropwise to the mixture on an ice bath with magnetic stirring. After 10 min, 0.676 mL of 0.1 M ammonium persulfate and 1 M $LiClO_4$ in 1 M $H_2SO_4$ was added dropwise over the course of 10 min. The solution was kept shielded from light and on an ice bath, with magnetic stirring for 8 h during polymerization. The product was washed with ethanol and acetone to remove the residual oxidant, followed by rinsing several times with a large amount of water. The loading of polyaniline was ~70 wt%, and the total N content in PANi/G-O composite is ~10.5 wt%. After drying at 60 °C, the product was annealed at 850 °C under Ar protection (50 sccm) for 1 h, and then washed by

ethanol, then DI water for further use. The sample is labeled as PANi/RG-O.

### Characterization

Scanning electron microscopy (SEM) images were obtained with a field-emission scanning electron microscope (FESEM, JEOL JSM-6700F). The Brunauer–Emmett–Teller (BET) method was used to determine the specific surface area by measuring the adsorption of $N_2$ using an ASAP2020 volumetric adsorption analyzer (Micromeritics, U.S.A.). The surface chemical composition of the samples was determined by X-ray photoelectron spectroscopy (XPS) on a VG ESCALAB 250 spectrometer (Thermo Electron, U.K.), using an Al K$\alpha$ X-ray source (1486 eV).

All of the electrochemical tests were carried out in a standard three-electrode cell with a Pt plate as the counter electrode. The electrochemical cell was controlled with an Autolab PGSTAT302 electrochemical test system (Eco Chemie, The Netherlands). ORR tests were conducted in an $O_2$-saturated 0.1 M KOH electrolyte (Ag/AgCl reference electrode) on a rotating-disk electrode system, in which the rotational speed was varied from 100 to 3000 rpm with a scan rate of 10 mV $s^{-1}$. The electrolyte was bubbled with purified oxygen flow at around 140 sccm for about 30 min before every experiment. The oxygen flow was then kept constant at 140 sccm throughout the whole measurement. The working electrode was fabricated by casting the catalyst ink onto a 5 mm diameter glassy carbon electrode. To prepare the catalyst ink, 10 mg of the N-containing graphene sample was ultrasonically dispersed into 1 mL of 2-propanol containing a Nafion solution (5 wt%, DuPont). 20 μL of the catalyst ink was coated on the glassy carbon electrode and dried at 60 °C. The bare glassy carbon electrode was tested without catalyst casting for comparison. The commercial Pt-loaded carbon catalyst (Pt/C 20% on Vulcan XC-72R, E-TEK division, PeMEAS Fuel Cell Technologies) was also used for comparison.

## Results and discussion

In order to alter the identities of the N moieties, together with G-O, aniline, pyrrole, and ammonia gas are used as precursors for preparation of N-doped graphene as shown in Scheme 1. BN-RG-O is prepared from the N-RG-O 550 °C sample, with B covalently bonded with pyridinic N (Fig. S1†). SEM images of N-RG-O 850 °C and N-RG-O 1000 °C samples are shown in Fig. 1. The SEM images show that the morphologies of the N-RG-O 850 °C and N-RG-O 1000 °C samples are similar, but both of them show platelets in crumpled conformations with more edges appearing to be exposed compared with pristine G-O. These edge planes, like stacked pallets, provide appropriate locations for N to incorporate into the graphite matrix.[21] The total surface area of N-RG-O 850 °C was measured to be 350 $m^2$ $g^{-1}$ by the BET method, larger than that of the freeze-dried G-O specimen which was measured to be 280 $m^2$ $g^{-1}$. Thermal annealing of G-O sheets has been reported to cause significant atomic rearrangement leading to a highly disordered graphene-like structure.[22]

SEM images clearly show the wrinkles on graphene layers. Chemical reactivity on or near the wrinkles may be enhanced due to the appearance of mid-gap states which lead to additional strong increase of chemisorption energy.[23] Therefore, the wrinkles and disordered structure along with the increased surface area could facilitate the adsorption of $O_2$, which would be advantageous for ORR applications.

The XPS broad scan shows the presence of C, N, and O in the N-RG-O and Ppy/RG-O samples, and also confirms that boron was successfully introduced into the BN-RG-O samples (Fig. 2). The oxygen content in BN-RG-O after annealing at 1000 °C is higher than that of Ppy/RG-O, N-RG-O 850 °C or N-RG-O 1000 °C. The high annealing temperature is known to increase the probability for oxygen incorporation as carbonyl groups and ether rings; therefore, high temperature annealing does not

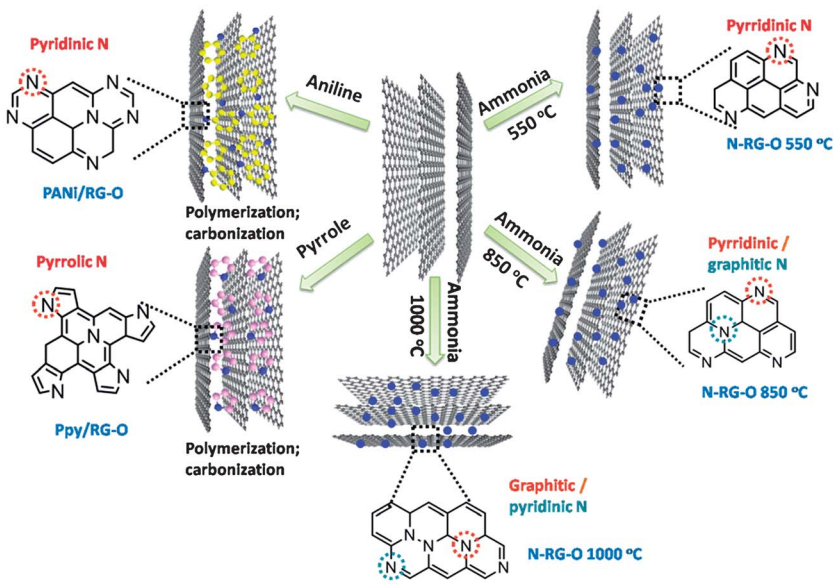


**Scheme 1** Schematic diagram for preparation of N doped graphene with different N states. N-RG-O 550, 850, and 1000 °C are prepared by annealing of G-O powder at temperatures of 550 °C, 850 °C, and 1000 °C under a $NH_3$·N precursor. PANi/RG-O and Ppy/RG-O are prepared by annealing of PANi/G-O and Ppy/G-O composites at 850 °C.

 

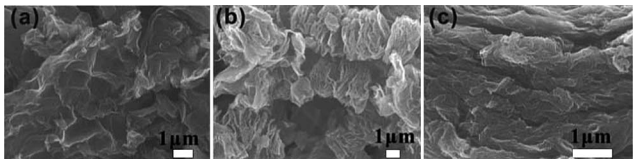


**Fig. 1** SEM images of G-O (a), N-RG-O 850 °C (b) and N-RG-O 1000 °C (c).

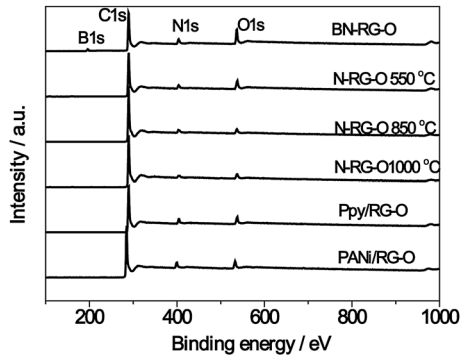


**Fig. 2** XPS survey scan of Ppy/RG-O, PANi/RG-O, BN-RG-O and N-RG-O samples annealed at various temperatures.

always decrease oxygen content.[22] The relative elemental compositions of the different catalysts were analyzed from XPS spectra. The total surface N content in N-RG-O is around 5.2 to 5.6%, lower than that of Ppy/RG-O which is around 6.6%. BN-RG-O exhibited the highest N content at 8.3%; however, the oxygen content was also higher than the other catalysts (Table 1).

The deconvoluted high-resolution N1s spectra of N-RG-O, Ppy/RG-O and BN-RG-O are shown in Fig. 3. Generally, there are several N-containing functional groups in N-doped carbon which can be identified by the bonding state of the N atom in the composite.

These groups include pyridinic N (~398.7 eV), pyrrolic N (~400.3 eV), quaternary N (~401.2 eV), and *N*-oxides of pyridinic N (~402.8 eV).[24,25] Pyridinic N refers to N atoms at the edges of graphene planes, where each N atom is bonded to two carbon atoms and donates one p-electron to the aromatic π system.[8,15,17] Pyrrolic N atoms are incorporated into five-membered heterocyclic rings, which are bonded to two carbon atoms and contribute two p-electrons to the π system. Quaternary N atoms are incorporated into the graphene layer and substitute carbon atoms within the graphene plane. *N*-oxides of pyridinic N, pyridinic-$N^+$–$O^-$, are N atoms bonded to two carbon atoms and one oxygen atom. The pyridinic and pyrrolic N are always located at the graphitic edge, whereas quaternary N can be both "edge-N" and "bulk-like-N".[25]

Analysis of the N1s peaks around 398, 400, and 401 eV provides the relative atomic ratios of each type of N species. In order to reveal the chemical states of N in detail, the N1s spectra were decomposed into different peaks according to different aforementioned chemical states of N. The binding energy and relative composition ratio of N in the different catalysts are summarized in Table 2. It is worthwhile to note that the pyridinic N content appears to decrease as the annealing temperature is increased to 1000 °C. This is because the pyridinic groups are not

**Table 1** Surface species concentration for various N-containing catalysts summarized by XPS results[a]

| | Species concentration (atomic%) | | |
|---|---|---|---|
| | C | O | N |
| BN-RG-O | 78.10 | 13.60 | 2.91 |
| Ppy/RG-O | 86.30 | 6.10 | 6.60 |
| PANi/RG-O | 84.31 | 8.33 | 7.36 |
| N-RG-O 550 °C | 84.90 | 9.70 | 5.40 |
| N-RG-O 850 °C | 89.70 | 4.70 | 5.60 |
| N-RG-O 1000 °C | 90.10 | 4.70 | 5.20 |

[a] Hydrogen is not taken into account for the calculation.

thermally stable and they convert to pyrrolic- and graphitic N groups at higher annealing temperatures. The N atomic ratio in Ppy/RG-O before annealing is around 10%; however, the N atomic ratio remains 6.6% after annealing, which is still higher than in the N-RG-O based catalyst. 84% of the N in Ppy/RG-O is present in the form of pyrrolic-N. No deconvoluted peak at 401 eV can be resolved for Ppy/RG-O annealed at 850 °C, indicating that the pyrrolic-N in Ppy is stable and does not transform to graphitic-N even under high temperature annealing. For the BN-RG-O sample annealed at 1000 °C, 68.43% N atoms are in the form of pyridinic N, and most of the pyridinic N are covalently bonded with B as determined from analysis of the B1s spectra (Fig. S1†). This may prohibit the transformation of pyridinic N to graphitic N in graphene, although the BN-RG-O samples are annealed under 1000 °C. It has been reported that B and N co-doped carbon has improved catalytic activity compared with N-doped carbon.[26–28] The $O_2$ molecules bind

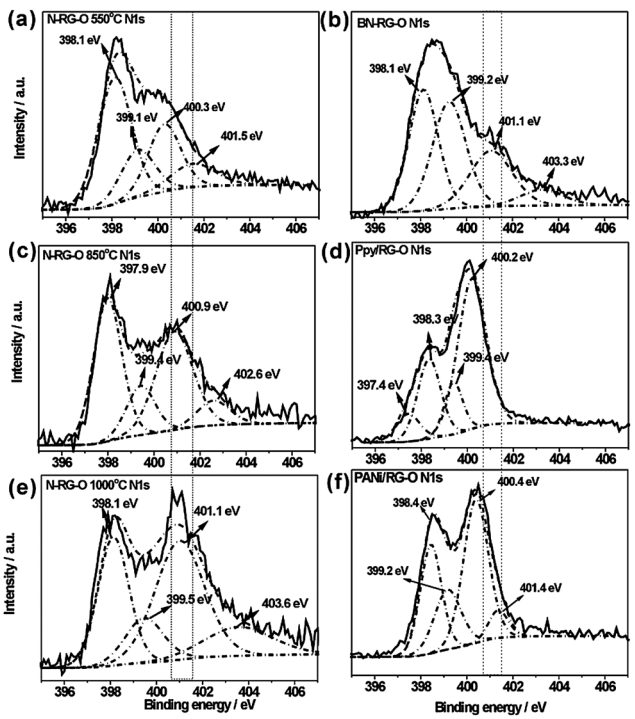


**Fig. 3** N1s spectra of N-RG-O 550 °C (a), BN-RG-O (b), N-RG-O 850 °C (c), Ppy/RG-O (d), N-RG-O 1000 °C (e) and PANi/RG-O (f).

**Table 2** Detailed breakdown of N1s spectra from Ppy/RG-O, BN-RG-O and N-RG-O samples under different annealing temperatures from XPS analysis, indicating peak position and relative atomic ratios of N species[a]

| | N-RG-O 550 °C | | N-RG-O 850 °C | | N-RG-O 1000 °C | |
|---|---|---|---|---|---|---|
| N species | Peak position/eV | % N | Peak position/eV | % N | Peak position/eV | % N |
| Pyridinic | 398.1 | 3.48 | 397.9 | 4.03 | 398.1 | 0.96 |
| Pyrrolic | 400.3 | 1.29 | 399.4 | 0.38 | 399.5 | 2.76 |
| Quaternary | 401.5 | 0.63 | 400.9 | 0.98 | 401.1 | 1.12 |
| Pyridine oxide | — | — | 402.6 | 0.21 | 403.6 | 0.36 |
| | BN-RG-O | | Ppy/RG-O | | PANi/RG-O | |
| N species | Peak position/eV | % N | Peak position/eV | % N | Peak position/eV | % N |
| Pyridinic | 398.1 | 1.99 | 397.4–399.4 | 2.94 | 398.4, 399.2 | 3.58 |
| Pyrrolic | 399.2 | 0.49 | 400.2 | 3.66 | 400.4 | 3.29 |
| Quaternary | 401.1 | 0.34 | — | — | 401.4 | 0.49 |
| Pyridine oxide | 403.3 | 0.09 | — | — | — | — |

[a] Hydrogen is not taken into account for the calculation.



easily to N–B–N complexes at zigzag edges due to the strong inter-atomic attraction between neighboring B and N. Therefore, N–B–N-dominated zigzag edges could give improved ORR activity.[26] However, it is important to note that, in this study, boron is bonded to pyridinic N, thus B does not replace C but instead covalently bonds with one pyridinic N.

Although there are reports that the introduction of N doping can effectively improve the ORR catalytic activity of carbon,[10,11] the identity and role of the electrocatalytically active center are still controversial as its contribution to catalytic activity is not well defined. Pyridinic-N modifies the band structure of carbon, raising the density of $\pi$ states near the Fermi level and lowering the work function. However, pyridinic-N is not an effective promoter for ORR activity of carbon, as evidenced by the sluggish ORR activity as reported in our previous study on N-doped CVD grown graphene,[17] while, the relative electronegativity of graphitic N atoms reduces the electron density on the adjacent C nuclei, which helps electrons transfer from the adjacent C to N atoms, and N backdonates electrons to adjacent C $p_z$ orbitals.[29] The donation and backdonation processes not only facilitate $O_2$ dissociation on the adjacent C atoms, but also help forming a strong chemical bond between O and C.[29] For example, surprisingly high ORR activity has been achieved with only 2.8% N content on N-RG-O, from which the authors claimed that quaternary-type N species played the most important role in ORR activity.[11]

We acquired rotating disk electrode voltammograms to investigate the electrocatalytic properties of N-RG-O, PANi/RG-O, and Ppy/RG-O in comparison with bare Pt, glassy carbon and commercial 20% Pt/C catalysts. Fig. 4a shows the linear voltammetric scans of different catalysts in an $O_2$-saturated 0.1 M KOH electrolyte with a rotation rate of 2500 rpm. In terms of limiting current density, the highest value was obtained on N-RG-O 1000 °C, followed by bare Pt, PANi/RG-O, Ppy/RG-O, BN-RG-O, and bare glassy carbon, but still lower than that of 20% Pt/C. The polarization curves of N-RG-O 1000 °C at different potentials and rotation speeds are shown in Fig. 4b. The linear voltammetric curves of different catalysts under various electrode rotating rates ranging from 500 to 3000 rpm, along with their corresponding ORR performance in the diffusion and kinetically limited regions, were evaluated using Koutecky–Levich (K–L) plots as shown in Fig. S2–7†. The K–L plot presents a linear relationship between the reciprocal of measured

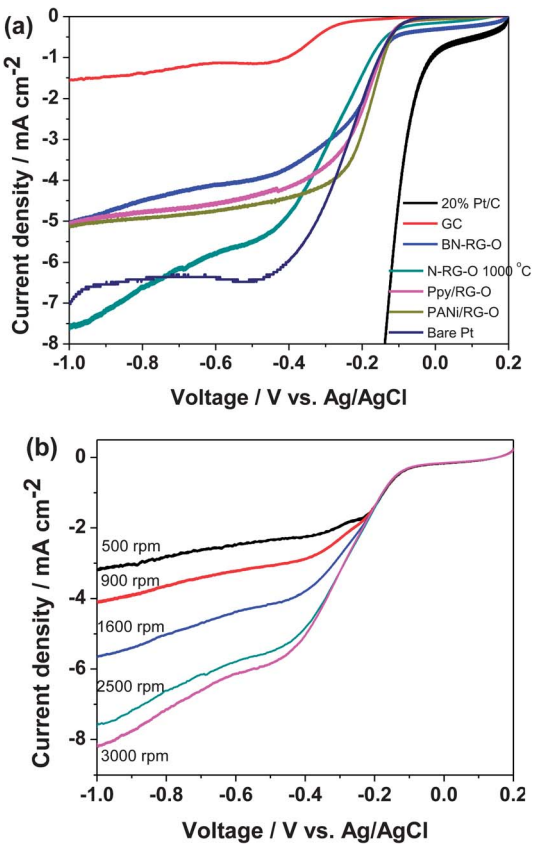


**Fig. 4** (a) Linear sweep voltammograms for N-RG-O 1000 °C, bare GC electrode, PANi/RG-O Ppy/RG-O, BN-RG-O, bare Pt electrode and 20% Pt/C electrodes in $O_2$ saturated 0.1 M KOH (scan rate: 10 mV $s^{-1}$, rotation rate 2500 rpm). (b) Linear sweep voltammograms for N-RG-O 1000 °C with a rotation rate from 500 to 3000 rpm.

current density ($j$), kinetic current density ($j_k$), and reciprocal of the square root of rotation speed ($\omega$) as follows:

$$\frac{1}{j} = \frac{1}{j_k} + \frac{1}{j_l^{diff}} \quad (1)$$

where $j_k$ is the kinetic current density and $j_l^{diff} = B\omega^{1/2}$ is the limiting diffusion current density, $B$ is the Levich constant, and $\omega$ is the rotation rate of the electrode.

As seen from Fig. 5a, all of the K–L plots of rotating disk electrode curves from different catalysts show a linear relationship between $1/j$ and $\omega^{-1/2}$ at a potential of −0.95 V. Furthermore, the Levich slopes show minor variations at applied potentials for all the samples, which is an indication of first order ORR kinetics with respect to the concentration of dissolved $O_2$.[30,31] By extrapolation of the K–L line to the origin of the plot, or as $\omega$ approaches $\infty$, the $y$-intercept yields the kinetic current density, while the $x$-intercept indicates catalytic activity towards ORR.[24]

The number of electrons transferred for each oxygen molecule can be calculated from the Levich constant *via* the following equation:

$$B = 0.62nFD^{2/3}\nu^{-1/6}C_o \quad (2)$$

where $F$ (Faradic constant) = 96486 C mol$^{-1}$, $D$ is the diffusion coefficient of $O_2$ in the electrolyte ($1.73 \times 10^{-5}$ cm$^2$ s$^{-1}$) in 0.1 M KOH, $\nu$ is the kinematic viscosity of the electrolyte (0.01 cm$^2$ s$^{-1}$), $C_o$ is the concentration of oxygen ($1.21 \times 10^{-6}$ mol L$^{-1}$), and $n$ is the number of exchanged electrons per oxygen molecule.

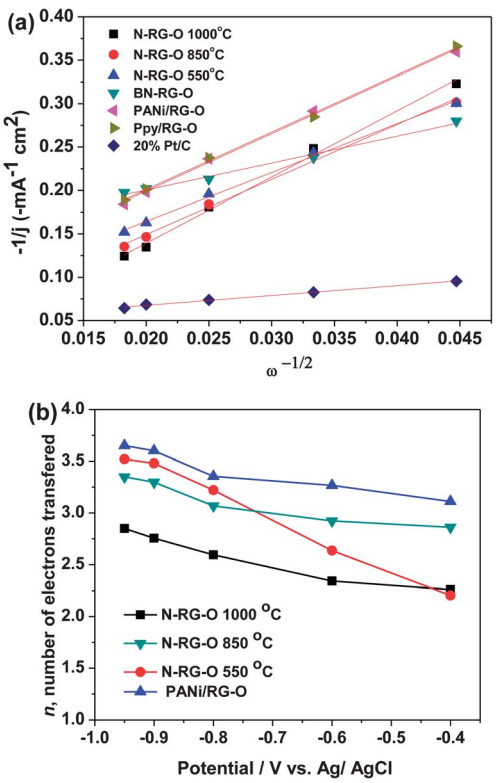


**Fig. 5** (a) Koutecky–Levich plots for BN-RG-O, PANi/RG-O, PPy/RG-O, N-RG-O 550 °C, N-RG-O 850 °C, N-RG-O 1000 °C and commercial 20% Pt/C in 0.1 M KOH at −0.95 V *vs.* Ag/AgCl. (b) The number of electrons transferred per $O_2$ molecule at different potentials based on the Koutecky–Levich equation for N-RG-O and PANi/RG-O.

According to eqn (1) and (2), the number of electrons transferred ($n$) and $j_k$ can be obtained from the slope and the intercept of the K–L plots. The number of electrons transferred at different potentials in the ORR process for the N-RG-O 550 °C, N-RG-O 850 °C, N-RG-O 1000 °C, and PANi/RG-O samples are shown in Fig. 5b. The number of electrons transferred in the ORR process for the N-RG-O 550 °C, N-RG-O 850 °C, and N-RG-O 1000 °C samples are 3.52, 3.35, and 2.85, respectively, while the electron transfer numbers in 20% Pt/C, BN-RG-O, PANi/RG-O and Ppy/RG-O are 3.98, 3.45, 3.65 and 3.63 respectively. For N-RG-O prepared from annealing under $NH_3$, the limiting current densities are much larger than those prepared from annealing of graphene/N-containing polymer composites. Increasing the N-RG-O annealing temperature will raise the limiting current density, but shift the ORR to a 2e$^-$ mechanism. The primary difference between the N-RG-O 550 °C, N-RG-O 850 °C, and N-RG-O 1000 °C samples is the different types of N species present. N-RG-O 1000 °C contains more graphitic N than N-RG-O 550 °C and N-RG-O 850 °C, while N-RG-O 850 °C has a higher pyridinic N component than N-RG-O 550 °C and N-RG-O 1000 °C. The N-RG-O 1000 °C sample exhibited largest limiting current density (Fig. S8†), as well as the largest graphitic N component with an atomic ratio of 1.08% (Table 1). Ppy/RG-O and PANi/RG-O have comparable ORR activities and relative limiting current density and onset potential. However, from voltages of −0.15 to −0.9 V, the kinetic current density of PANi/RG-O is larger than that of Ppy/RG-O. The N-doping state of Ppy/RG-O is dominated by pyrrolic N with an atomic percentage of 3.66%, while pyridinic N is the primary N bonding state in PANi/RG-O with an atomic percentage of 3.58% (Table 2). One reasonable interpretation is that pyridinic N is more catalytically active than pyrrolic N during the ORR process. The ORR activity of BN-RG-O is lower than that of PANi/RG-O and Ppy/RG-O as seen from the smaller kinetic current density over the voltage range of −0.2 to −0.9 V. B–N co-doped carbon in a N–B–N complex at zigzag edges should give improved ORR activity.[26] However, in this study, B does not replace C but rather covalently bonds with pyridinic-N atoms, which prohibits the transformation of pyridinic N to graphitic N due to the covalent bonding of B to N. In this case, even though the BN-RG-O sample is annealed at 1000 °C, the graphitic N content is still low with an atomic percentage of 0.34%. Comparing the RDE curves of BN-RG-O with N-RG-O 1000 °C, it is reasonable to conclude that a higher limiting current density of N-RG-O than BN-RG-O might be due to the abundance of graphitic N atoms in N-RG-O, compared with pyridinic N-dominated BN-RG-O.

Graphitic N atoms have been reported to serve as ORR catalytic sites both experimentally and theoretically due to the reduced adsorption energy.[19,25,32] Graphitic carbon nitrides show promise for applications in fuel cell and metal free heterogeneous catalysis, as recently reviewed by Zheng *et al.*[33] Kim *et al.* found that graphene edge structures would become more catalytically active after introduction of graphitic N; furthermore, such structures would not only enhance the first electron transfer rate, but also show preference for the 4e$^-$ reduction pathway.[19] The graphitic N at the graphene edge may catalyze ORR through

a ring-opening of the cyclic C–N bond, which results in the formation of pyridinic N.[19,26] However, as a marker of edge plane exposure, pyridinic N and pyrrolic N are always located at edge sites, which are chemically active themselves.[25,33] Thus, it is uncertain as to whether or not the pyridinic or pyrrolic N provides actual active sites for promoting ORR, or whether the reaction is simply more favorable due to the abundance of highly active edges and/or defect sites.[25,34] Comparing a series of as-prepared catalysts shows that the graphitic N-dominated catalysts have higher catalytic activity with larger limiting current density than that of pyrrolic or pyridinic N-dominated N-containing catalyst.

The enhancement of ORR performance should be ascribed to the increased electron density and electron donating properties resulting from the valence electrons donated by the N dopant. Pyridinic N could reduce the adsorption energy of $O_2$,[16] whereas graphitic N is capable of electroreduction of $O_2$ to $H_2O_2$ *via* adsorbed OOH intermediates through a $2e^-$ way.[35] The electron transfer number as calculated from K–L curves also shows that N-RG-O 1000 °C is 2.85 per $O_2$ molecule. It is also worthwhile to note that, although N-RG-O 1000 °C has a larger portion of graphitic N atoms compared with N-RG-O 850 °C or N-RG-O 550 °C, the onset potential of N-RG-O 1000 °C is much smaller than that of N-RG-O 850 °C and N-RG-O 550 °C, while the slope of N-RG-O 1000 °C K–L curves indicates the reduced derivation in the number of electrons transferred per oxygen molecule. This further confirms that N-RG-O 850 °C and N-RG-O 550 °C samples, with an abundance of pyridinic-N species, tend to drive ORR through a $4e^-$ mechanism, while N-RG-O 1000 °C gives the highest limiting current density. Although PANi/RG-O and Ppy/RG-O have highest N atomic ratio, they show even worse catalytic activity than that of the as-prepared N-RG-O based catalyst. This phenomenon indicates that the total atomic content of N in the metal-free, graphene-based catalyst did not play an important role in the ORR process.

## Conclusions

N-doped graphene is a promising material for use as an ORR catalyst, but a deeper understanding of the relationship between the type and concentration of N species and catalyst activity is needed. In this study, we prepared N-doped RG-O by annealing of G-O under ammonia and found that this material tends to show superior ORR catalytic performance to catalysts produced by annealing of G-O with N containing polymer composites, perhaps due to the considerable content of both pyridinic N and graphitic N. Annealing of PANi/RG-O and Ppy/RG-O gives products containing predominately pyridinic N and pyrrolic N species, respectively. Most importantly, the electrocatalytic activity of N-containing metal-free catalysts is highly dependent on the graphitic N content while pyridinic N species improve the onset potential for ORR. However, the total atomic content of N in the metal-free, graphene-based catalyst did not play an important role in the ORR process. Graphitic N can greatly increase the limiting current density, while pyridinic N species might convert the ORR reaction mechanism from a $2e^-$ dominated process to a $4e^-$ dominated process.

## References


1 R. M. Darling and J. P. Meyers, *J. Electrochem. Soc.*, 2003, **150**, A1523.
2 J. Greeley, I. E. L. Stephens, A. S. Bondarenko, T. P. Johansson, H. A. Hansen, T. F. Jaramillo, J. Rossmeisl, I. Chorkendorff and J. K. Norskov, *Nat. Chem.*, 2009, **1**, 552.
3 L. Zhang, J. J. Zhang, D. P. Wilkinson and H. J. Wang, *J. Power Sources*, 2006, **156**, 171.
4 S. Maldonado and K. J. Stevenson, *J. Phys. Chem. B*, 2005, **109**, 4707.
5 Z. H. Sheng, L. Shao, J. J. Chen, W. J. Bao, F. B. Wang and X. H. Xia, *ACS Nano*, 2011, **5**, 4350.
6 V. Nallathambi, J. W. Lee, S. P. Kumaraguru, G. Wu and B. N. Popov, *J. Power Sources*, 2008, **183**, 34.
7 E. J. Biddinger, D. von Deak and U. S. Ozkan, *Top. Catal.*, 2009, **52**, 1566.
8 K. A. Kurak and A. B. Anderson, *J. Phys. Chem. C*, 2009, **113**, 6730.
9 C. V. Rao, C. R. Cabrera and Y. Ishikawa, *J. Phys. Chem. Lett.*, 2010, **1**, 2622.
10 L. T. Qu, Y. Liu, J. B. Baek and L. M. Dai, *ACS Nano*, 2010, **4**, 1321.
11 D. S. Geng, Y. Chen, Y. G. Chen, Y. L. Li, R. Y. Li, X. L. Sun, S. Y. Ye and S. Knights, *Energy Environ. Sci.*, 2011, **4**, 760.
12 K. P. Gong, F. Du, Z. H. Xia, M. Durstock and L. M. Dai, *Science*, 2009, **323**, 760.
13 L. Y. Feng, Y. Y. Yan, Y. G. Chen and L. J. Wang, *Energy Environ. Sci.*, 2011, **4**, 1892.
14 H. R. Byon, J. Suntivich and Y. Shao-Horn, *Chem. Mater.*, 2011, **23**, 3421.
15 K. R. Lee, K. U. Lee, J. W. Lee, B. T. Ahn and S. I. Woo, *Electrochem. Commun.*, 2010, **12**, 1052.
16 N. P. Subramanian, X. G. Li, V. Nallathambi, S. P. Kumaraguru, H. Colon-Mercado, G. Wu, J. W. Lee and B. N. Popov, *J. Power Sources*, 2009, **188**, 38.
17 Z. Q. Luo, S. H. Lim, Z. Q. Tian, J. Z. Shang, L. F. Lai, B. MacDonald, C. Fu, Z. X. Shen, T. Yu and J. Y. Lin, *J. Mater. Chem.*, 2011, **21**, 8038.
18 P. Wang, Z. K. Wang, L. X. Jia and Z. L. Xiao, *Phys. Chem. Chem. Phys.*, 2009, **11**, 2730.
19 H. Kim, K. Lee, S. I. Woo and Y. Jung, *Phys. Chem. Chem. Phys.*, 2011, **13**, 17505.
20 W. S. Hummers and R. E. Offeman, *J. Am. Chem. Soc.*, 1958, **80**, 1339.
21 F. Jaouen, F. Charreteur and J. P. Dodelet, *J. Electrochem. Soc.*, 2006, **153**, A689.
22 A. Bagri, C. Mattevi, M. Acik, Y. J. Chabal, M. Chhowalla and V. B. Shenoy, *Nat. Chem.*, 2010, **2**, 581.
23 D. W. Boukhvalov and M. I. Katsnelson, *J. Phys. Chem. C*, 2009, **113**, 14176.
24 Z. Chen, D. Higgins and Z. W. Chen, *Carbon*, 2010, **48**, 3057.
25 E. J. Biddinger and U. S. Ozkan, *J. Phys. Chem. C*, 2010, **114**, 15306.
26 T. Ikeda, M. Boero, S. F. Huang, K. Terakura, M. Oshima, J. Ozaki and S. Miyata, *J. Phys. Chem. C*, 2010, **114**, 8933.
27 S. F. Huang, K. Terakura, T. Ozaki, T. Ikeda, M. Boero, M. Oshima, J. Ozaki and S. Miyata, *Phys. Rev. B: Condens. Matter Mater. Phys.*, 2009, **80**, 235410.
28 J. Ozaki, N. Kimura, T. Anahara and A. Oya, *Carbon*, 2007, **45**, 1847.
29 D. H. Deng, X. L. Pan, L. A. Yu, Y. Cui, Y. P. Jiang, J. Qi, W. X. Li, Q. A. Fu, X. C. Ma, Q. K. Xue, G. Q. Sun and X. H. Bao, *Chem. Mater.*, 2011, **23**, 1188.
30 Y. Gochi-Ponce, G. Alonso-Nunez and N. Alonso-Vante, *Electrochem. Commun.*, 2006, **8**, 1487.
31 M. Pattabi, R. H. Castellanos, R. Castillo, A. L. Ocampo, J. Moreira, P. J. Sebastian, J. C. McClure and X. Mathew, *Int. J. Hydrogen Energy*, 2001, **26**, 171.
32 R. L. Liu, D. Q. Wu, X. L. Feng and K. Mullen, *Angew. Chem., Int. Ed.*, 2010, **49**, 2565.
33 Y. Zheng, J. Liu, J. Liang, M. Jaroniec and S. Z. Qiao, *Energy Environ. Sci.*, 2012, **5**, 6717.
34 M. Jain, S. H. Chou and A. Siedle, *J. Phys. Chem. B*, 2006, **110**, 4179.
35 D. H. D. Higgins, Z. Chen and Z. W. Chen, *Electrochim. Acta*, 2011, **56**, 1570.